Electronic Supplementary Material (ESI) for Nanoscale.
This journal is © The Royal Society of Chemistry 2020

Supporting Information

An underwater writable and heat-insulated paper with robust fluorine-free superhydrophobic coatings

Zhibin Jiao,[a] Wencai Chu,[a] Linpeng Liu,[a] Zhengzhi Mu,[a] Bo Li,[a] Ze Wang,[a] Zhiwei Liao,[b] Yuchen Wang,[b] Hao Xue,[a] Shichao Niu,*[ab] Saihua Jiang,[bc] Zhiwu Han,*[a] and Luquan Ren[a]

[a] Key Laboratory of Bionic Engineering, Ministry of Education, Jilin University, Changchun 130022, China.

[b] Department of Materials Science and Engineering, University of Pennsylvania, Philadelphia 19104, United States.

[c] School of Mechanical and Automotive Engineering, South China University of Technology, Guangzhou, 510641, China.

The reaction between Si-OH and HMDS is given as follows:

$$2 - OH + (CH_3)_3\, SiNHSi\,(CH_3)_3 \rightarrow 2 - O - Si\,(CH_3)_3 + NH_3 \uparrow \tag{S1}$$

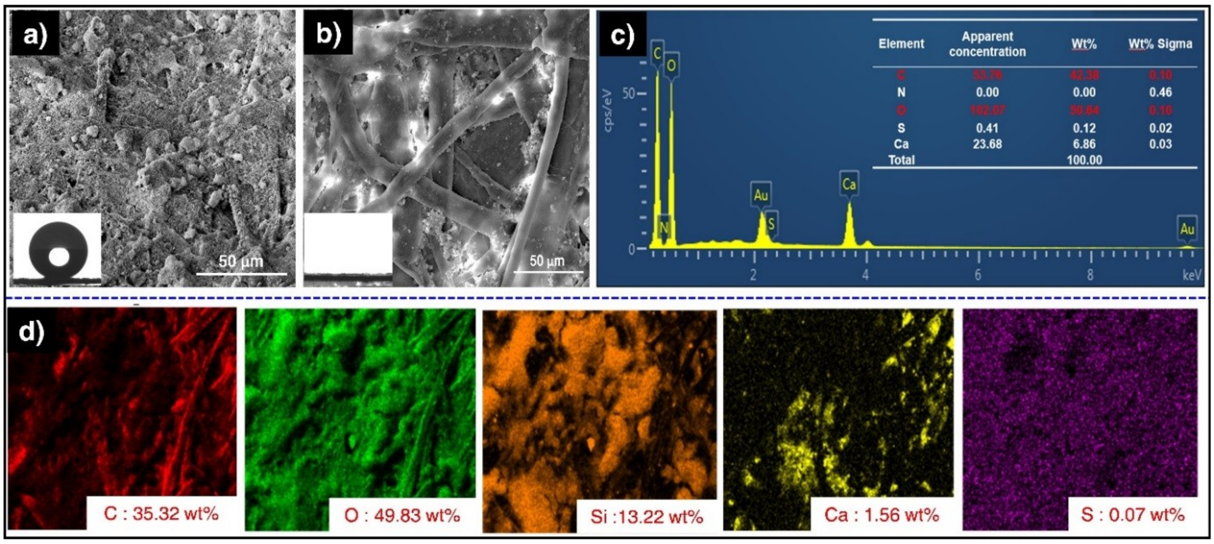

Fig. S1 (a) SEM images of the BSP after spraying, showing more distinct rough surface. The inset picture displays the superhydrophobic properties of the BSP. (b) SEM image of the conventional paper before spraying, showing a rough surface in micrometer scale. The inset picture exhibits the superhydrophilic properties of the conventional paper. (c) EDS spectra of the conventional paper. (d) FESEM-EDS mapping of the BSP.

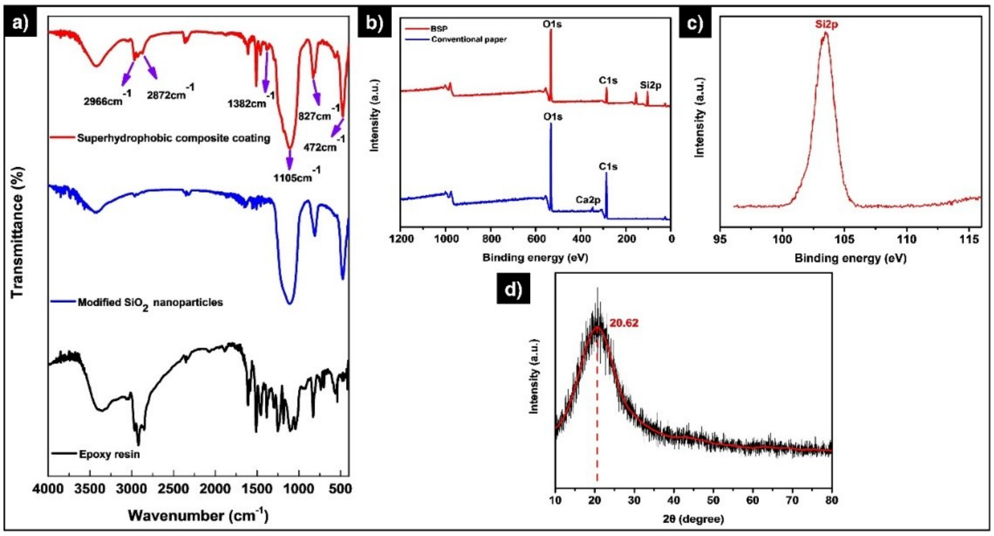

Fig. S2 Analysis of the chemical binding and elemental composition of the BSP. (a) FTIR image of the superhydrophobic composite coating, modified SiO_2 NPs and ER. (b) XPS full-scan spectra of the BSP and conventional paper. (c) Si 2p high-resolution scan spectra of the BSP. (d) XRD patterns of the superhydrophobic composite coating.

As shown in Fig.S2(a), from the FTIR curve of ER, it has -OH stretching vibration absorption peak and $-CH_2$ asymmetric stretching vibration absorption peak at 3357 cm^{-1} and 2919 cm^{-1}, respectively. And the stretching vibration peaks of the benzene ring skeleton are also found at 1614 cm^{-1} and 1510 cm^{-1}. In addition, the C=O stretching vibration absorption peak is observed at 1181 cm^{-1}. The stretching vibration peak of the epoxy group is also observed at 916 cm^{-1}. From the FTIR curve of the modified SiO_2 NPs, the stretching vibration absorption peak for the -OH groups appear at 3437 cm^{-1}, which may be caused by the absorption of moisture in the air. The $Si-CH_3$ stretching vibration absorption peaks are also found at the 2964 cm^{-1} and 2904 cm^{-1}. Furthermore, the Si-O-Si asymmetric stretching vibration absorption peak is observed at 1093 cm^{-1}. And the Si-O-Si symmetrical stretching vibration and bending vibration absorption peaks are observed at 807 cm^{-1} and 472 cm^{-1}, respectively. Additionally, from the FTIR curve of the superhydrophobic composite coating, a characteristic peak similar to the modified SiO_2 NPs appears at 3424 cm^{-1}, that is, the stretching vibration absorption peak for -OH groups. These small amounts of -OH groups incorporated inside the coating do not affect the superhydrophobic properties. The absorption bands at 2966 cm^{-1} (Si-CH_3 symmetric stretching vibration), 2872 cm^{-1} (Si-CH_2) and 1382 cm^{-1} (Si-CH_2 bending vibration) can be also found, respectively. Besides, the stretching vibration peaks of the benzene ring skeleton appeared at 1616 cm^{-1} and 1508 cm^{-1}, indicating that ER is successfully introduced into the composite coating. In particular, the stretching vibration peak of the epoxy group at 916 cm^{-1} in the composite coating has disappeared, which indicates that ER has completely cured. Moreover, the absorption bands at 1105 cm^{-1}(Si-O-Si asymmetric stretching vibration), 827 cm^{-1}(Si-O-Si symmetric stretching vibration) and 472 (Si-O-Si bending vibration) cm^{-1} are also observed, respectively. It shows that part of hydrophilic silanol groups (Si-OH) on the surface of SiO_2 NPs are successfully replaced by the hydrophobic -$OSi(CH_3)_3$ groups. The above results indicate that the composite coating is successfully endowed with hydrophobic groups and contains ER and SiO_2 NPs.

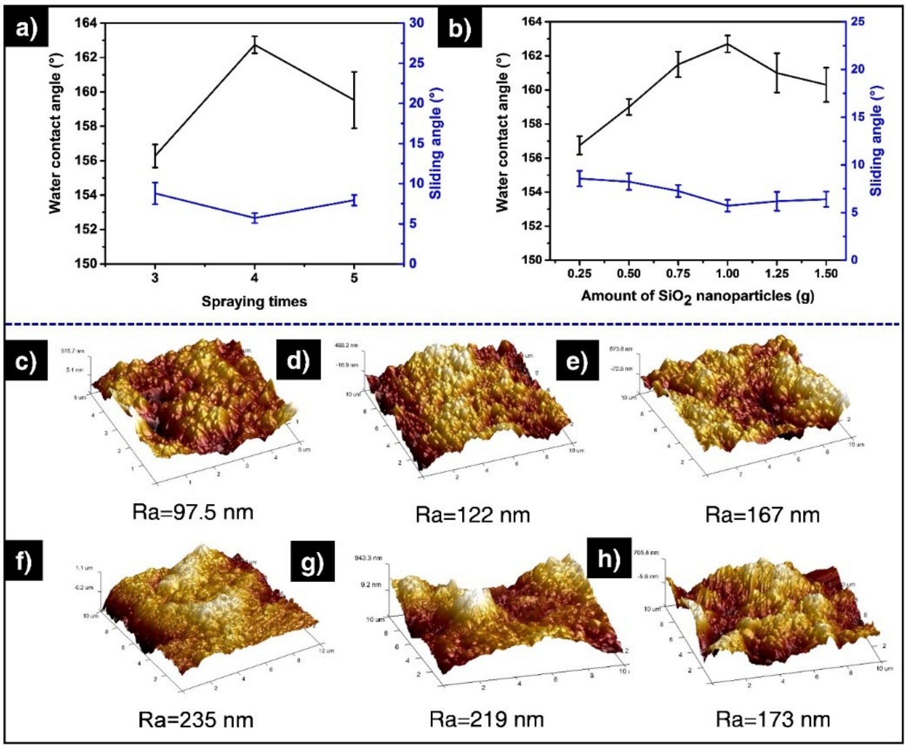

Fig. S3 (a) WCAs and SAs of the BSP as a function of different times for spraying SiO_2 NPs. In this case, the amount of SiO_2 NPs, ER and its curing agent are 1.0 g, 0.3 g and 0.1 g, respectively. The BSP exhibits the optimal superhydrophobicity with a WCA of 162.7 ± 0.49° and a SA of 5.72 ± 0.62° when spraying four times. (b) WCAs and SAs of the BSP as a function of various amount of SiO_2 NPs. In this case, the amount of ER and its curing agent of are 0.3 g and 0.1 g, respectively. The spraying process are repeated for four times. The optimal superhydrophobicity is achieved when the amount of SiO_2 NPs is 1.0 g, showing a WCA of 162.7 ± 0.49° and a SA of 5.72 ± 0.62°. AFM images of surface roughness on the top of the BSP consisting of different amounts of SiO_2 nanoparticles. (c) 0.25 g, (d) 0.5 g, (e) 0.75 g, (f) 1.0 g, (g) 1.25 g, (h) 1.5 g. When the amount of SiO_2 NPs is 1.0 g, the optimum surface roughness with about 235 nm is obtained.

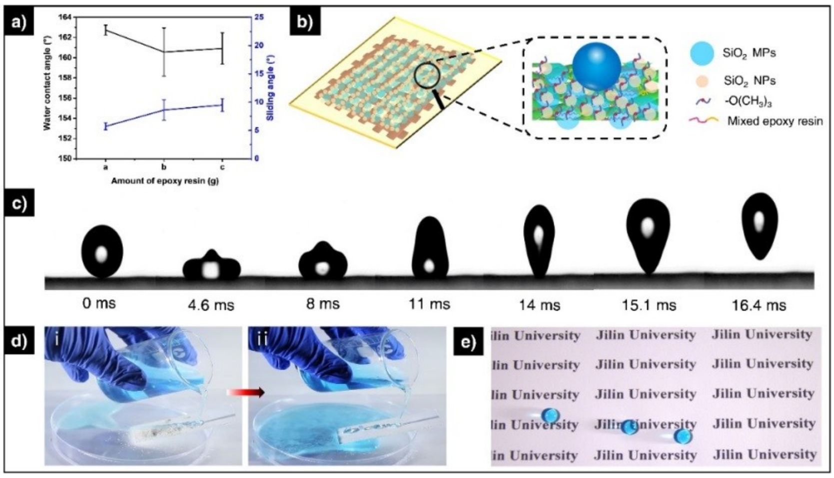

Fig. S4 Surface wettability, self-cleaning and optical transparence performances of the BSP. (a) WCAs and SAs of the BSP as a function of the amount of ER. The amount of ER and its curing agent are 0.3 g and 0.1 g, 0.6 g and 0.2 g, 0.9 g and 0.3 g, respectively, which are represented by a, b, and c, respectively. The optimal superhydrophobic performance with a WCA of 162.7 ± 0.49° and a SA of 5.72 ± 0.62° is obtained when the amount of ER and its curing agent is 0.3 g and 0.1 g, respectively. (b) Schematic illustration of the superhydrophobic mechanism of the BSP with hierarchical micro-/nanostructures. (c) Selected snapshot of the bounce dynamics of a water droplet impacting on the BSP surface. The water droplets with a radius of about 1.40 mm are dropped down from a height of 30 mm. Upon impacted with the interface of the BSP, the water droplet spreads and presents a pancake shape at approximately *t*= 4.6 ms. Then, the water droplet retracts and completely bounces off the BSP at approximately *t*=16.4 ms. (d) Digital images present the process that fine sand particles on the BSP are washed away by the water with methyl blue. (e) Optical transparency of the BSP. It is fabricated by first printing and then spraying. The optical transparency of the BSP is attributed to the hierarchical structures and SiO_2 NPs with the size smaller than the wavelength of visible light, which both increase the optical path lengths and reduce the Fresnel reflection. Thereby, it decreases light scattering and improve transparency in the visible wavelength range.[1,2] Additionally, the water droplets present on the surface in a spherical form.

References

1 Z. Han, Z. Jiao, S. Niu and L. Ren, *Prog. Mater. Sci.*, 2019, **103**, 1–68.

2 S. Chattopadhyay, Y. F. Huang, Y. J. Jen, A. Ganguly, K. H. Chen and L. C. Chen, *Mater. Sci. Eng. R Reports*, 2010, **69**, 1–35.

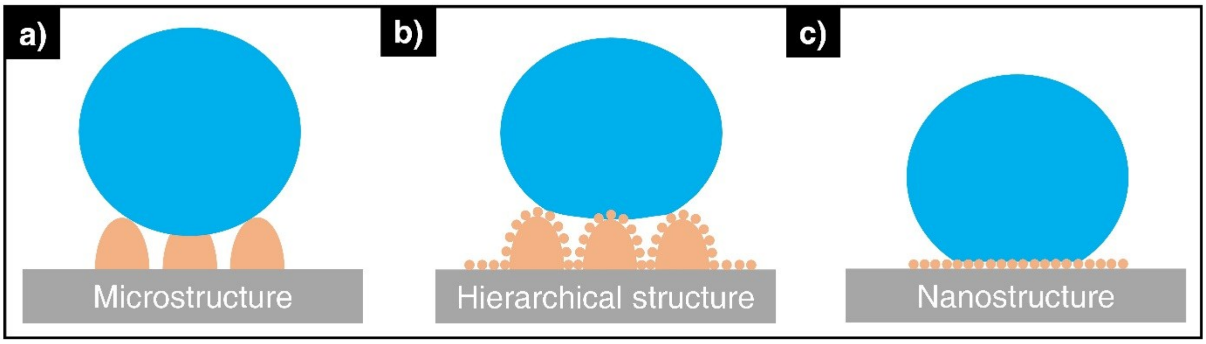

Fig. S5 Schematic of the simplified wetting models for three surface structures. (a) Microstructured surface. (b) Hierarchical structured surface. (c) Nanostructured surface.

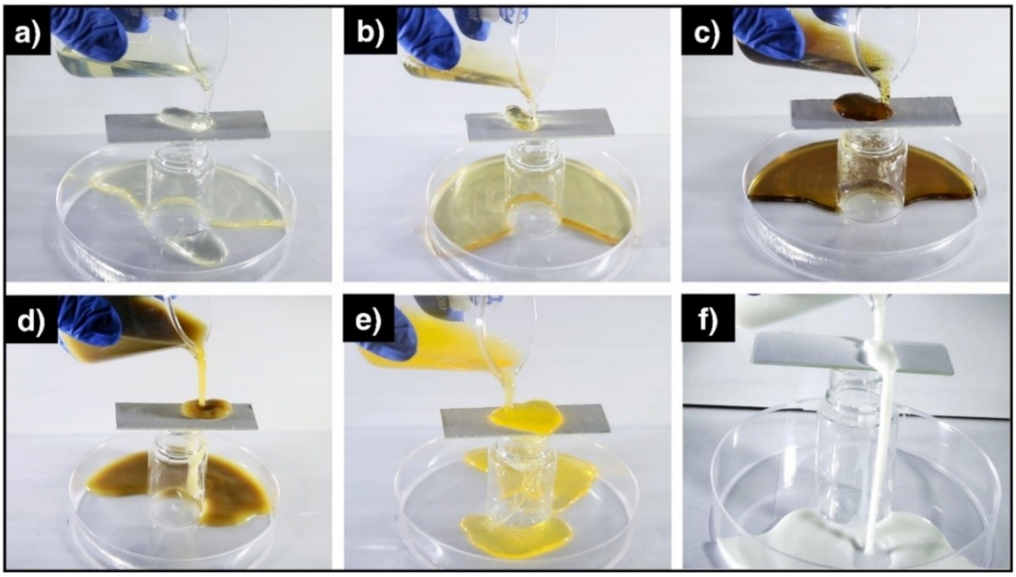

Fig. S6 Six different beverages are (a) Green tea, (b) Red tea, (c) Coca Cola, (d) Coffee, (e) Orange juice, and (f) Milk. They were poured onto the BSP surface to test the liquid-repellence property.

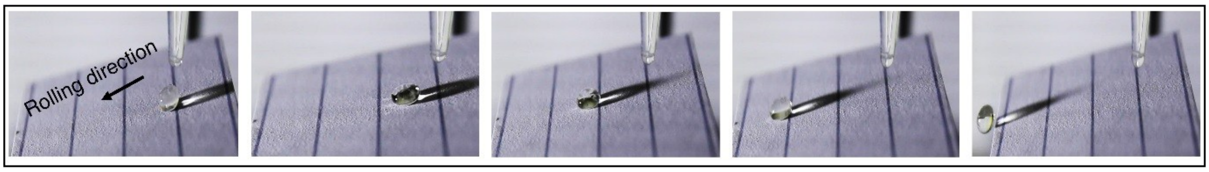

Fig. S7 Rolling process of the green tea on the BSP surface with an inclination angle of 15°

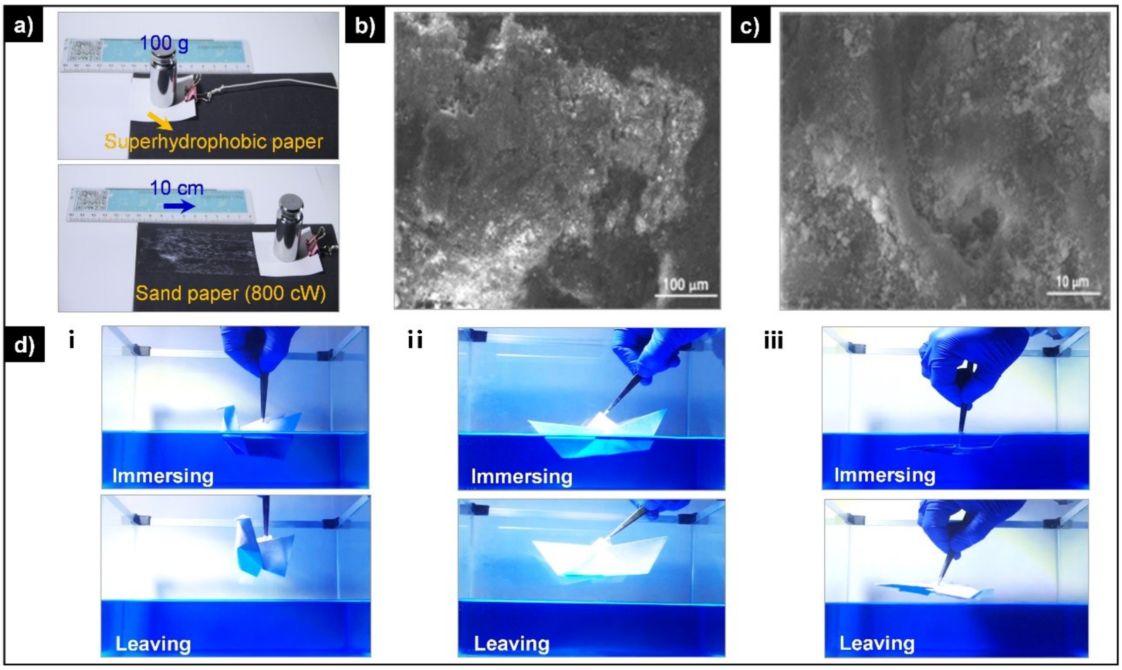

Fig. S8 Mechanical properties testing of the BSP. (a) The abrasion process of the BSP, where the BSP was placed on the sandpaper (800 cW) with 100 g load. Dragging once in the direction of the blue arrow is considered as one abrasion cycle. (b) and (c) SEM images of the BSP after abrasion test. (d) Origami folding testing of the BSP and the process from the immersing to leaving water, showing the superhydrophobic property after multiple folding processes.

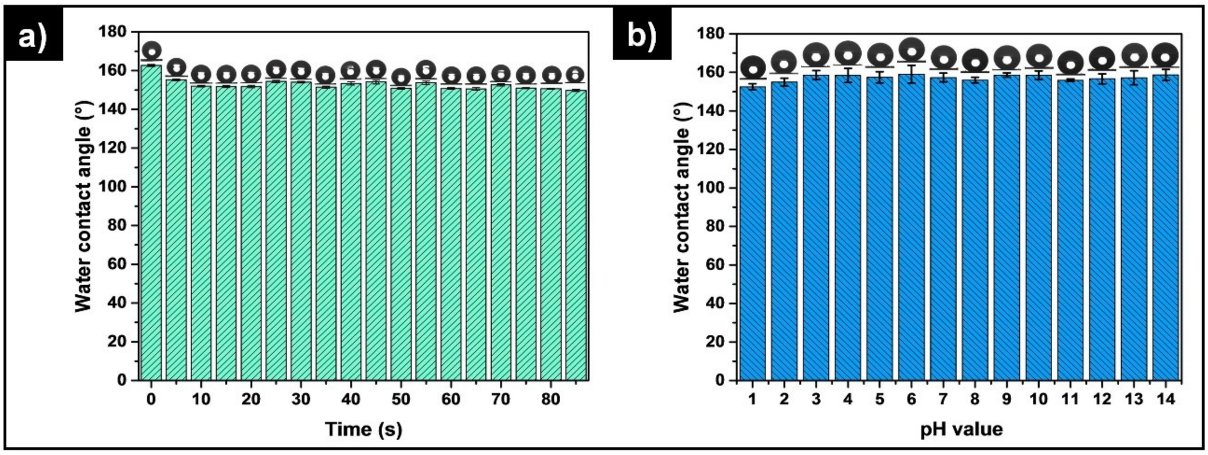

Fig. S9 Boiling water resistance and chemical stability test. (a) WCAs of the BSP as a function of the immersion time in boiling water. (b) The measured WCAs of the BSP after soaking in the corrosion solutions with the pH values varying from 1 to 14 for 3 min.

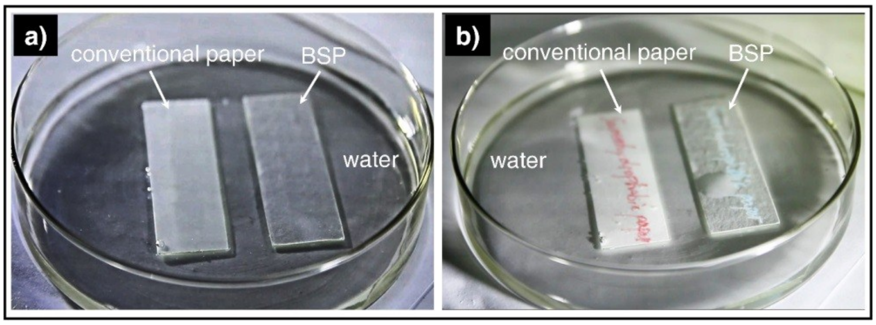

Fig. S10 The process of writing underwater on the BSP. (a) Conventional paper and the BSP are completely immerged in the glassware filled with water. It can be clearly seen that the BSP surface remains intact while that of the conventional paper has been completely wetted. (b) The image after writing words on surface of the conventional paper and the BSP, respectively. After writing, the words on the BSP surface is clearly visible. Its surface keeps normal while that of the conventional paper has been slightly damaged.

Movie S1 The bounce dynamics test of a water droplet impacting on the BSP surface.

Movie S2 The experiment of self-cleaning property of the BSP. The fine sand particles on the BSP surface were washed away by the water with methyl blue, and the surface did not leave any traces of water.

Movie S3 Flushing test for the paper with printed words by the water with methyl blue. This paper was divided into two parts: the coated part (left) and uncoated part (right). Obviously, the coated part did not leave any traces of water compared with the uncoated part of the paper.

Movie S4 The repellency tests of different beverages, including green tea, red tea, Coca Cola, coffee, orange juice and milk, respectively.

Movie S5 Abrasion test of the BSP.

Movie S6 Origami folding test on the mechanical stability of the BSP with different shapes including the paper crane, boat and airplane. The surface of the folded BSP did not leave any traces of water during the process from immersing to leaving water, after undergoing multiple folds.

Movie S7 Underwater writable test of the conventional paper and the BSP.